AIChE WILEY InterScience DISCOVER SOMETHING GREAT

Experimental and Modeling Study of the O_2-Enrichment by Perovskite Fibers

Christof Hamel
Max Planck Institute for Dynamics of Complex Technical Systems Sandtorstr. 1, D-39106 Magdeburg, Germany

Andreas Seidel-Morgenstern
Max Planck Institute for Dynamics of Complex Technical Systems Sandtorstr. 1, D-39106 Magdeburg, Germany, and Otto von Guericke University, Institute of Process Engineering, Universitätsplatz 2, D-39106 Magdeburg, Germany

Thomas Schiestel
Fraunhofer Institute of Interfacial Engineering and Biotechnology (IGB), Nobelstr. 12, D-70569 Stuttgart, Germany

Steffen Werth
Uhde GmbH, Friedrich-Uhde-Str. 15, D-44141 Dortmund, Germany

Haihui Wang, Cristina Tablet, and Jürgen Caro
Hannover University, Institute of Physical Chemistry and Electrochemistry, Callinstr. 3-3A, D-30167 Hannover, Germany

DOI 10.1002/aic.10934
Published online July 17, 2006 in Wiley InterScience (www.interscience.wiley.com).

The production of O_2-enriched air (OEA) using dense mixed conducting perovskite hollow fiber membranes was studied experimentally and theoretically. The fibers were prepared by phase inversion spinning followed by sintering. A mathematical model was developed based on the mass balances for the OEA side, the O_2-depleted air side and the hollow fiber itself to simulate the O_2-enrichment. Based on the experiments and the model, the mass transport in the mixed conducting material was quantified using Wagner's theory. Furthermore, 3-D plots of broad parameter fields were calculated to estimate optimal operation conditions for a maximum O_2-enrichment. The results elucidate that a required O_2 concentration in the OEA, and the production rate can be adjusted by controlling the operation parameters, such as temperature, air pressure differences and sweep air flow rates. The long term operation (800 h) indicates that the perovskite hollow fiber membranes offer a promising potential for the industrial OEA production. © 2006 American Institute of Chemical Engineers *AIChE J,* 52: 3118–3125, 2006
Keywords: oxygen enrichment, mixed conducting membranes, hollow fibers, perovskite membranes, oxygen separation, reactor modeling, mass transfer, Wagner's theory

Introduction

There is a large potential application of O_2-enriched air (OEA) in order to perform enhanced combustion. O_2-enrichment of up to 30% has been demonstrated to provide benefits in combustion efficiency and pollution reduction.[1] OEA with 30–50% O_2 is also used in a number of industrial processes, for example, in ammonia synthesis, the Claus process and the fluidized catalytic cracking (FCC) catalyst regeneration.[1,2] Another application field of OEA is the most efficient utilization of methane in high-temperature furnaces or cement kilns.[2]

There are different existing technologies for the production

Correspondence concerning this article should be addressed to H. Wang at haihui.wang@pci.uni.hannover.de.

© 2006 American Institute of Chemical Engineers

of OEA. Mainly mixing air with pure O_2 is applied. Such a system usually requires pure O_2 supply equipment, a control skid and a sparger which is used to mix the pure O_2 and air well. The current commercial pure O_2 supply equipment is based on cryogenic fractionation technology or pressure swing adsorption (PSA). However, these techniques require high-capital and operational costs. Membrane separations have drawn great attention in air separation. Polymeric membranes that have sufficient selectivity to O_2 and high-flux are intensively studied for O_2-enrichment. However, since normal polymeric membranes generally have a low separation factor (O_2:N_2 in 5–8 range) at a considerable permeability, a single-stage polymeric membrane is limited to produce O_2 purity up to 50%. Although, high O_2 purity and permeability can be achieved by increasing the feed flow rate, reducing the membrane thickness or by increasing the pressure difference, all of these actions increase the separation cost.[3] Furthermore, a high-pressure difference of about 9.0×10^5 Pa (10×10^5 Pa on the feed side, and 1.0×10^5 Pa on the permeate side) is needed for polymeric membranes to get reasonable O_2 fluxes, leading to high costs for the air compression. Another problem is that polymeric membranes cannot be used for the recovery of heat from exhaust gas, which prevents their use in high-temperature reactions or process applications.

Membrane development represents a frontier research area in chemical engineering, materials science and materials chemistry. The breakthrough in the wide application of organic polymer membranes in dialysis, natural gas treatment and treatment of refinery gas streams became possible through the availability of hollow fiber membranes. Consequently, increasing activities can be observed in the preparation of oxygen ion conducting membranes in hollow fiber geometry. Examples are the pioneering articles from the groups of Li[4-8] and Galavas[9,10] as well as the articles by Schiestel et al.,[11] Trunec,[12] Luyten et al.,[13] and Tablet et al.[14] showing that ceramic fibers with thin wall can be prepared by phase inversion spinning followed by sintering. The development of perovskite hollow fiber membranes is expected to trigger a similar development like it was observed in the field of hollow fiber organic polymer membranes.

In our previous article,[15] we proposed a novel technique to produce OEA using a mixed ion and electron conducting (MIEC) perovskite membrane. Such perovskite membranes are promising to apply in the field of chemical processing, including partial oxidation of natural gas to syngas (POM),[16-19] oxidative coupling of methane to value-added products such as ethane/ethylene,[20-22] selective oxidation of hydrocarbons[23-25], and power generation.[26,27] Under a slight air pressure difference ($1.0 - 2.0 \times 10^5$ Pa) oxygen can be transported through the MIEC perovskite membrane in the form of oxygen ions from the high to the low air pressure side. Simultaneously, electrons are transported in the opposite direction to maintain the electric neutrality. The permeated oxygen increases the O_2 concentration in the sweep air forming OEA on the low-pressure side. This technique offers several advantages for the oxygen enrichment:

1. Perovskite membranes combine the *in situ* O_2 supply, and the mixing of the permeated O_2 with air in one unit, thus simplifying the process for the O_2-enrichment and reducing the operational and capital costs.

2. Compared with organic polymer hollow fiber membranes, the perovskite hollow fiber membrane requires a relatively lower pressure difference ($1.0 - 2.0 \times 10^5$ Pa) across the membrane and can work at elevated temperatures, thus, allowing high-temperature heat exchange.

3. Perovskite membranes exhibit 100% selectivity for oxygen,[4,10,28,29] and there is no correlation between permeability and selectivity for perovskite membranes, as it is the case for polymer membranes. Increasing the pressure difference leads to an increase of oxygen permeation flux while the selectivity remains stable (100%). Polymeric membranes also transport noble or inert gases like Ar or CO_2, which can be disadvantageous depending on the process design.

4. The stability and operational safety problems of perovskite membranes, which happen at low oxygen partial pressures, such as under the syngas atmospheres, are not relevant in the proposed O_2-enrichment process because both sides of the perovskite membranes are exposed to an oxidizing atmosphere (air).[15]

In continuation of the ongoing research, the production of OEA using dense MIEC perovskite hollow fibers was studied experimentally and theoretically in this article. A mathematical model simulating the process of OEA production using the $BaCo_xFe_yZr_zO_{3-\delta}$ (BCFZ, $x + y + z = 1.0$) hollow fibers has been developed. A comprehensive analysis was conducted to investigate the effects of various factors on the performance of the permeator. The results of modeling and experiments were compared. The derived model was then used to simulate the OEA production in a broad parameter range of air pressure difference, sweep-gas fluxes and temperatures to assess optimal operation conditions. This work intends to develop a more in-depth understanding of the OEA production process using the BCFZ hollow fibers in order to provide guidance regarding design of a perovskite module for the O_2-enrichment under industrial conditions.

Experimental

We applied hydrolysis of the corresponding metal nitrates by an ammonium hydroxide solution to get the precursor BCFZ. The precursor was mixed with a solution of polysulfone in an organic solvent and ball milled. The slurry was spun through a spinneret and the green BCFZ perovskite fiber obtained was cut into 50 cm pieces before sintering them in a hanging geometry. During the sintering above 1,200°C, the length and the diameter of the green fiber was reduced from an initial length of 50 cm and an outer diameter of ~0.175 cm to a final length of ~32 cm, and an outer diameter of around 0.1 cm.

In preliminary experiments the permeation of the hollow fiber perovskite membrane using He as the sweep gas was tested in a high-temperature gas permeation cell[14] at (1) different O_2-partial pressures which were obtained by mixing different ratios of nitrogen and oxygen (2) different temperatures between 700°C and 850°C. Air or synthetic air of different ratios of nitrogen and oxygen with a flow rate of 150 cm^3/min was fed to the shell side, and pure He (99.995 %) flowed on the core side of the membrane. The total pressure in the experiments is 1.2×10^5 Pa. The core side partial pressure of oxygen will change from inlet to outlet in these experiments. Thus, average values of both partial pressures have been used in this analysis to calculate the oxygen flux.

An O_2-enrichment was studied in a high-temperature perme-

ator.[15] The two ends of the hollow fiber membrane were sealed by two silicon rubber rings. Preheated air was fed 100 cm^3/min to the shell side and different air pressures were obtained by adjusting the needle valve on the outlet of air. The air pressures on the shell side varied between 1.5×10^5 Pa and 4.0×10^5 Pa. 10 – 150 cm^3/min preheated air was fed to the core side, and the air pressure was fixed at 1.036×10^5 Pa. Due to the air pressure difference between the shell side and the core side, the oxygen on the shell side permeates through the hollow fiber membrane to the core side and mixes with air to form OEA. The oxygen permeation flux, can be calculated as

$$J_{O_2} = \frac{F_{air,inlet} \times (C_{O_2,\text{outlet}} - C_{O_2,inlet})}{S \times (100 - C_{O_2,outlet})} \tag{1}$$

where $F_{air,inlet}$ (cm^3/min) is the air flow rate at the inlet on the core side; $C_{O_2,inlet}$ (%) is the fed O_2 concentration in air, $C_{O_2,outlet}$ (%) is the O_2 concentration at the outlet of the core side; and S (cm^2) is the effective membrane surface area of the hollow fiber for the oxygen permeation. The flow rates in the experiment are measured at the standard temperature and pressure. For the determination of the effective membrane area S, the following formula was used

$$S = \frac{2\pi L(r_2 - r_1)}{\ln(r_2/r_1)} \tag{2}$$

with r_2 (cm) and r_1 (cm) denoting the outer and inner radius of the hollow fiber, respectively. L (cm) is the effective length. When 32 cm long hollow fibers in a 24 cm long oven were studied, only 16 cm were assumed as the effective fiber length L since from measuring the temperature profile of the oven it is known that only the inner 16 cm of the oven have a temperature > 500°C. In this study, the effective membrane surface area is calculated to be 3.50 cm^2.

The OEA production rate, R_{OEA}, is defined as

$$R_{OEA} = \left.\frac{F_{Outlet}}{S}\right|_{C_{O_2,outlet}} \quad \text{with} \quad C_{O_2,outlet} > C_{O_2,inlet} \tag{3}$$

where F_{Outlet} (cm^3/min) is the flow rate at the outlet of the core side, which can be measured by soap film meter.

Model development

A gradient in the partial molar Gibbs free energy of oxygen, forming the essential driving forces for the mass transfer of oxygen in the considered material BCFZ, can be generated, for example, by:

1. Decreasing the oxygen partial pressure at one side of the hollow fiber by consumption of O_2 in a chemical reaction
2. Decreasing the O_2 partial pressure at one side of the hollow fiber by application of nonreactive sweep gases
3. Application of a significant difference in the total air pressure on both sides of the hollow fiber.

For the mathematical quantification of the mass transfer from shell to core side through the hollow fiber (see Figure 1) a one-dimensional (1-D), isothermal plug flow tubular reactor (PFTR) model was used. The derived model allows also the consideration and calculation for the usage of reactive sweep gases and a coupling, for example, with selective oxidation reactions, respectively. In this contribution air is used as a nonreactive sweep gas, that is, the reaction rate $\bar{r}$ is zero.

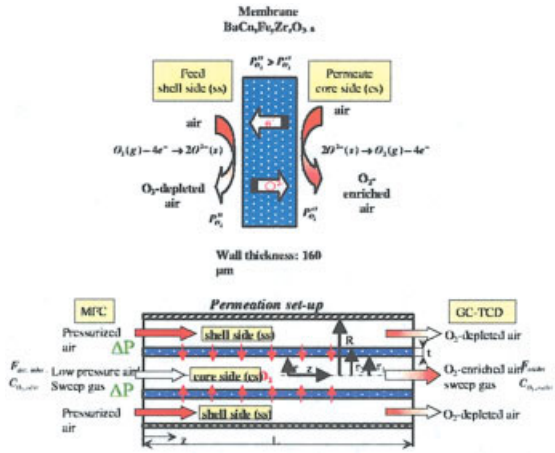

Figure 1. O_2-enrichment and the simulated configuration using perovskite fibers.

[Color figure can be viewed in the online issue, which is available at www.interscience.wiley.com.]

Under the following assumptions simplified mass balances can be formulated:

1. steady-state conditions
2. isothermal
3. ideal gas behavior
4. negligible axial and radial dispersion

Component and total mass balances on the shell side (ss) $r_2 < r < R$

$$\frac{d\dot{n}_i^{ss}}{dz} = -2 \cdot \pi \cdot r_2 \cdot J_i|_{r=r_2} \quad \text{with} \quad i = 1, N \tag{4}$$

$$\frac{d\dot{n}_{tot}^{ss}}{dz} = -2 \cdot \pi \cdot r_2 \cdot \sum_i J_i|_{r=r_2} \tag{5}$$

Oxygen flux through perovskite membranes $r_1 < r < r_2$.

The transport of oxygen ions in MIEC oxides is documented in manifold empirical, as well as physically founded approaches.[30] One approach based on thermodynamical mechanisms is the theory of Wagner[31, 32] assuming the gradient of the chemical potential of oxygen as the driving force for mass transfer. Thus, the Wagner approach was used to describe the transfer of oxygen ions through the BCFZ perovskite hollow fiber under study

$$J_{O_2} = \frac{D_{eff}}{4 \cdot n \cdot t} \cdot [(P_{O_2}^{ss})^n - (P_{O_2}^{cs})^n] \tag{6}$$

$$J_{O_2} = \frac{r_1}{r} \cdot J_{O_2}|_{r=r_1} \tag{7}$$

J_i of all other components is zero *Component and total mass balances on the core side (cs)* $0 < r < r_1$:

$$\frac{d\dot{n}_i^{cs}}{dz} = \pi \cdot r_1^2 \cdot \rho_{Bulk} \cdot \sum_j \nu_{ij} \cdot \bar{r}_j + 2\pi \cdot r_1 \cdot J_i|_{r=r_i} \qquad (8)$$

$$\text{with } i = 1, N; j = 1, M$$

The equations are coupled by the following boundary conditions

$$r = r_1 \quad J_{O_2} = J_{O_2}|_{r=r_1} \quad J_i = 0 \text{ for } i \neq O_2$$

$$p_{O_2}^{cs} = \frac{\dot{n}_{O_2}^{cs}}{\sum_i \dot{n}_i^{cs}} \cdot p_{tot}^{cs} = \frac{\dot{n}_{O_2}^{cs}}{\dot{n}_{tot}^{cs}} \cdot p_{tot}^{cs} \qquad (9)$$

$$r = r_2 \quad J_{O_2} = \frac{r_1}{r_2} \cdot J_{O_2}|_{r=r_1} \quad J_i \neq J_{O_2} = 0$$

$$p_{O_2}^{ss} = \frac{\dot{n}_{O_2}^{ss}}{\sum_i \dot{n}_i^{ss}} \cdot p_{tot}^{ss} = \frac{\dot{n}_{O_2}^{ss}}{\dot{n}_{tot}^{ss}} \cdot p_{tot}^{ss} \qquad (10)$$

The $\dot{n}_i$ and/or the J_i are specified for internal concentration profiles and finally the outlet concentration, calculated by numerical integration of the system of ordinary difference equations given by Eqs. 4–10 using standard techniques. This integration can be performed conveniently using MATLAB®.[33]

Results and Discussion

Estimation of mass-transfer parameters

The estimation and validation of mass-transfer parameters for the characterization, and the mathematical description of the hollow fiber properties are based on the performed experiments and the achieved data, respectively. The transport of oxygen ions is described by the theory of Wagner[31,32] assuming the gradient in the partial molar Gibbs free energy of oxygen is the driving force for mass transfer. When the oxygen ionic conductivity is much lower than the electronic one, the oxygen permeation flux through the MIEC membrane can be expressed well by Eq. 6 with an Arrhenius approach describing the temperature dependence of D_{eff} according to

$$D_{eff} = D_\infty \cdot e^{-(E_A/R \cdot T)} \qquad (11)$$

Figure 2 shows the temperature influence, and the dependency of the O_2 partial pressure on the oxygen permeation flux through the hollow fiber membrane using He as sweep gas. The comparison between the experimental data and the calculations using Eqs. 6 and 11, and the experimentally derived mass-transfer parameters reveal a sufficient agreement[11,14] and form the basis for further simulation studies. The parameters of the BCFZ hollow fiber membrane for OEA production and the operating condition, listed in Table 1, were employed in the simulation and experiments.

O_2-enriched air production

Figure 3 shows experimental and modeling results under variable air pressure differences. Both the experimental and modeling results show the same trend, that is, the oxygen permeation flux increases with enhancing the air pressure difference, thus promoting an increased driving force for oxygen permeation. The developed simple reduced 1-D-model, and the derived mass-transfer parameters for the hollow fiber agree very well with the experimental data set for the investigated parameter range of the given pressure difference. The production rate of OEA increases from 3.3 $cm^3/min \cdot cm^2$ to 5.0 $cm^3/min \cdot cm^2$ with the increase of O_2 concentration on the permeate side from 30% to 55% as the air pressure difference increases from 0.5×10^5 Pa to 3.0×10^5 Pa with a constant sweep air flow rate of 10 cm^3/min. The perovskite hollow fiber membrane can give an O_2 concentration of 38% with an O_2-enriched air production rate of 3.7 $cm^3/min \cdot cm^2$ applying only a pressure difference of 1.0×10^5 Pa. However, a commercial polymeric membrane with 25 μm thickness made from silicone rubbers only shows an oxygen permeation flux of ~0.11 $cm^3/min \cdot cm^2$ with an O_2 concentration of 35% under a pressure difference of 9.0×10^5 Pa.[34,35]

In Figure 4 the axial O_2 concentration profiles for the OEA

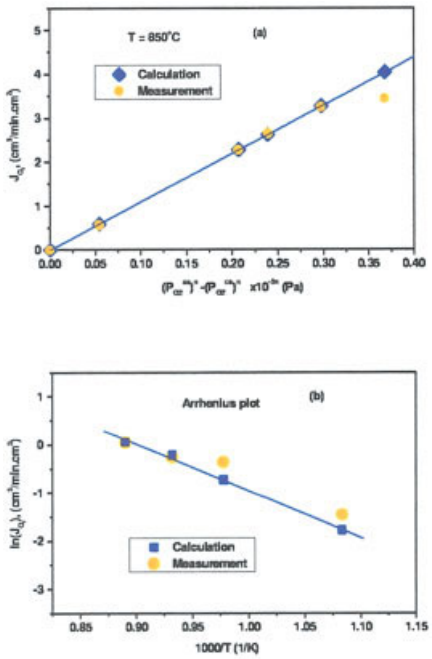

Figure 2. Experimental and simulated data using He as the sweep gas.

Air flow rate on the shell side: 150 cm^3/min, He flow rate on the core side: 30 cm^3/min. [Color figure can be viewed in the online issue, which is available at www.interscience.wiley.com.]

Table 1. Parameters Used in the Simulation and Experiments

Membrane area (cm^2)	$S = 3.5$
Outer radius (cm)	$r_2 = 0.042$
Inner radius (cm)	$r_1 = 0.026$
Thickness (cm)	$t = 0.016$
Effective membrane length (cm)	$L = 16$
Operation temperature (°C)	$T = 700–950$
Air flow rate on the shell side (cm^3/min)	100–150
Air flow rate on the core side (cm^3/min)	10–150
Air pressure difference (Pa)	$\Delta P = 0.5 - 10 \times 10^5$
Air pressure on the core side (Pa)	$P_{tot}^{cs} = 1.036 \times 10^5$
Activation energy in eq. (13) (kJ/mol)	$E_A = 113.9$

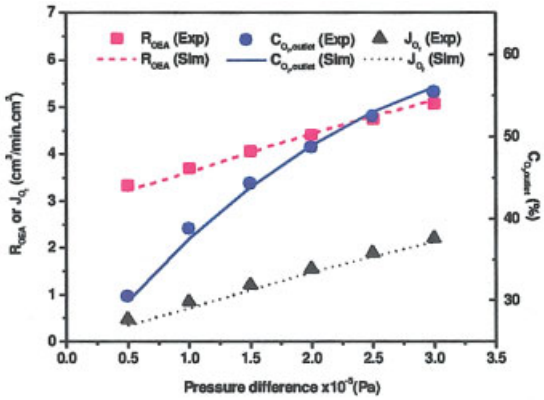

Figure 3. Dependence of pressure differences on the O_2-enrichment using a BCFZ fiber.

Air flow rate: Feed side = 100 cm^3/min; permeate side = 10 cm^3/min, T = 950°C. [Color figure can be viewed in the online issue, which is available at www.interscience.wiley.com.]

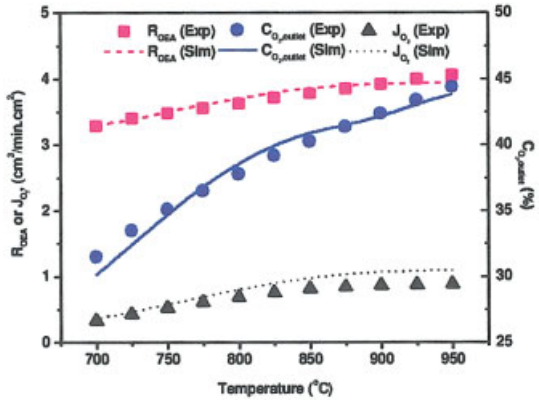

Figure 5. Temperature dependence on the oxygen enrichment using a BCFZ fiber.

Air flow rate: Feed side = 100 cm^3/min; Permeate side = 10 cm^3/min, pressure difference = 1.5×10^5 Pa. [Color figure can be viewed in the online issue, which is available at www.interscience.wiley.com.]

on the core side are illustrated as a function of the hollow fiber length for three selected pressure differences. The tubular permeation set-up constitutes of an open system of multiple molar fluxes (shell and core side) coupled over the oxygen permeation flux through the membrane. Thus, the oxygen permeation flux Jo_2, depends on the O_2 concentration and/or O_2 partial pressures on the core and shell sides, and this on each infinitesimal axial position. The estimated outlet concentrations as integral values correspond with the experimental data given in Figure 3.

As shown in Figure 4, an increasing pressure on the shell side (pressurized air) results in a higher driving force for the mass transfer, and in an increasing slope of the axial O_2 concentration profile. After half length of the hollow fiber, the change or the increase of the O_2 concentration is negligible. Thus, for the given pressure differences, the membrane could be shortened to achieve the same outlet concentrations. On the other hand, the length of 16 cm is also suitable to work at higher-pressure differences to increase the O_2 concentration on the permeate side (core side). The latter aspect is investigated

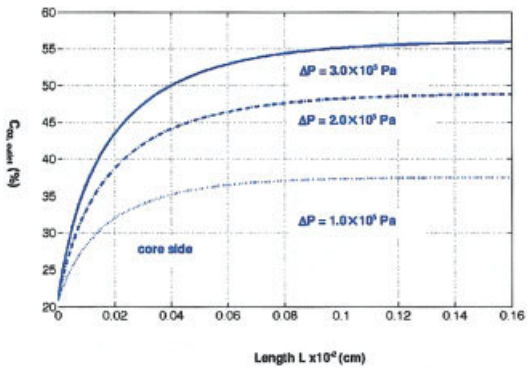

Figure 4. Axial profiles of the calculated O_2 concentration vs. hollow fiber length for three selected pressure differences at 950°C.

Air flow rate: Feed side = 100 cm^3/min, permeate side = 10 cm^3/min. [Color figure can be viewed in the online issue, which is available at www.interscience.wiley.com.]

in more detail in chapter "Evaluation of O_2-enrichement performance in a broader range of operation parameters".

Figure 5 shows the experimental and simulated oxygen permeation rate, OEA production rate and O_2 concentration vs. temperature under a fixed pressure difference of 1.5×10^5 Pa. The oxygen permeation rate increases with increasing temperature, which leads to the increase of the production rate of OEA and O_2 concentration on the permeate side. The simulations predict the same trend as the experiments, although the discrepancy between the simulated and experimental results is slightly higher at higher temperatures. This discrepancy, also seen in Figure 2, may be attributed to the assumption that the membrane thickness was assumed as 0.016 cm and was uniform through all the length of fiber. However, we cannot ensure that the membrane thickness is precisely 0.016 cm along the 30 cm fiber. Therefore, the slight difference in the membrane thickness along the fiber results in the inconsistency between modeling and experiment. Nevertheless, the simulated results are in good accordance with the experimental results.

Figure 6 shows the dependence of the air flow rate on the permeate side on the O_2-enrichment performance under a fixed air pressure difference of 1.5×10^5 Pa at 875°C. The oxygen permeation rate and the OEA production rate increase with increasing air flow rate on the permeate side. The reason is that the O_2 concentration was diluted significantly when the air flow rate on permeate side was increased. From Figure 6, it was also found that various O_2 concentrations required for the different industry processes can be obtained by adjusting the air flow rate on the permeate side.

Evaluation of O_2-enrichment performance in a broader range of operation parameters

A considerable advantage of modeling and simulation is the possibility of an effective and extensive calculation of broad parameter fields. The derived and validated 1-D model was used to simulate and assess the O_2-enrichment in an air separation module using BCFZ perovskite hollow fibers. In Figure 7 the oxygen permeation flux through the membrane Jo_2 (a), and the corresponding O_2 concentration of OEA (b), are illus-

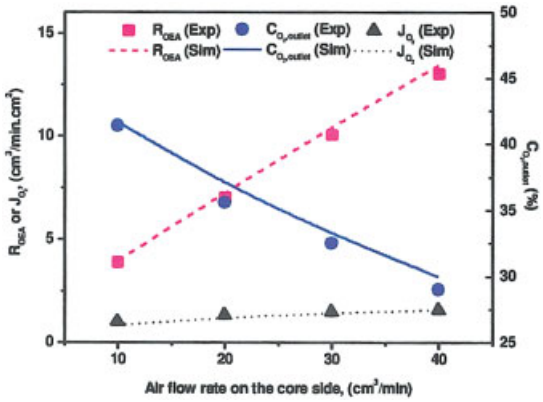

Figure 6. Dependence of air flow rate on the permeate side on the O_2-enrichment using a BCFZ fiber.

Air flow rate: Feed side = 100 cm^3/min, pressure difference = 1.5×10^5 Pa, T = 875°C. [Color figure can be viewed in the online issue, which is available at www.interscience.wiley.com.]

trated for a pressure difference of $\Delta P = 1.5 \times 10^5$ Pa vs. temperature and air flow rate on the permeate side. An enhancement of the process temperature increases the oxygen transport in the hollow fiber. An increase of the permeate flow

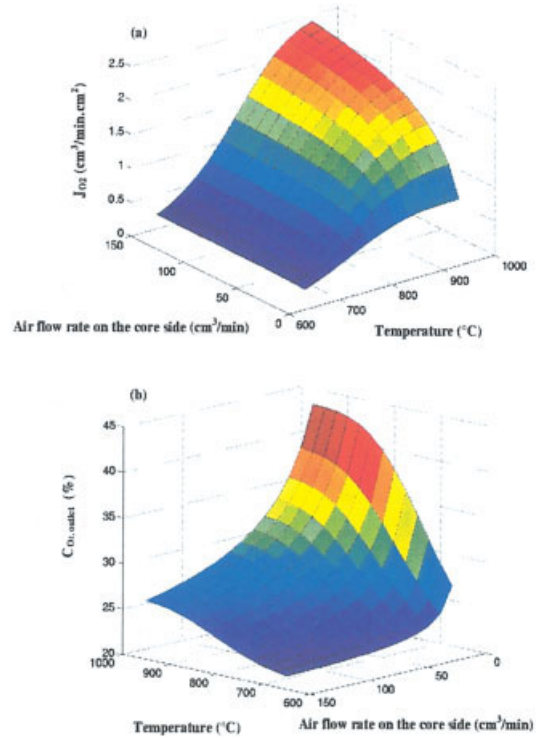

Figure 7. Influence of air flow rate on the permeate side and temperature on the OEA production: oxygen permeation flux through the membrane (a), and the resulting O_2 concentration in the permeate stream (b).

Air flow rate: Feed side = 100 cm^3/min; permeate side = 10 - 150 cm^3/min, T = 650-950°C, pressure difference = 1.5×10^5 Pa. [Color figure can be viewed in the online issue, which is available at www.interscience.wiley.com.]

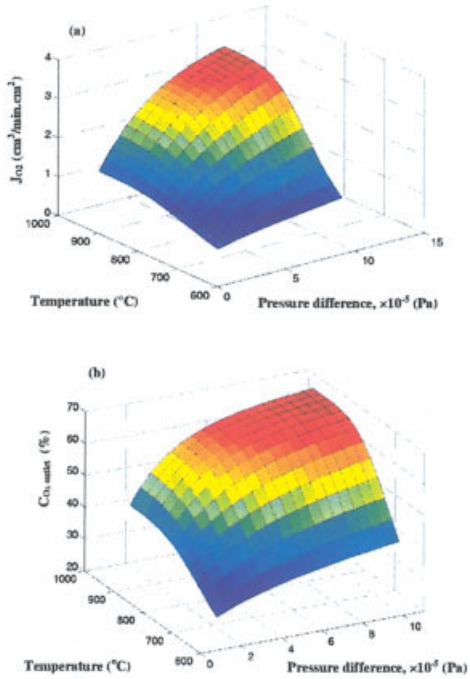

Figure 8. Influence of the pressure difference and temperature on the OEA production: oxygen permeation flux through the membrane (a) and the resulting O_2 concentration in the permeate stream (b).

Air flow rate: Feed side = 100 cm^3/min; permeate side = 10 cm^3/min, T = 650 - 950°C, pressure difference = 1.5 - 10×10^5 Pa. [Color figure can be viewed in the online issue, which is available at www.interscience.wiley.com.]

rate (sweep gas) leads to an increase of the driving force and, thus, to enhanced mass transfer (Figure 7a), but also to a decrease of the O_2 concentration in the permeate due to dilution.

An interesting possibility to enhance the gradient in the partial molar Gibbs free energy of oxygen is the application of higher differences in the total pressures. The oxygen permeation flux through the membrane (a), and the corresponding O_2 concentration of OEA (b), as a function of temperature and pressure difference are shown in Figure 8 for a constant air flow rate on the permeate side of 10 cm^3/min. An increase of the pressure difference leads to a pronounced enhancement of the oxygen flux and the oxygen concentration, respectively. The highest oxygen flux (a) of 3.3 $cm^3/min{\cdot}cm^2$ was observed for T = 950°C and $\Delta P = 10 \times 10^5$ Pa in the range covered (air flow rate: feed side = 100 cm^3/min; permeate side = 10 cm^3/min). Compared to the increase of fluxes based on increasing the sweep gas flow rate (Figure 7), the application of using higher total pressure gradients does not cause product dilution. The obtained O_2 concentrations of OEA of approximately 60% for relatively moderate pressure differences ($\Delta P = 4 \times 10^5$ Pa) and process temperatures (T = 850°C) are interesting. A further increase of Jo_2 for favorably lower-temperatures (T = 850°C) can be achieved by using increased sweep gas flow rates (sweep gas: permeate side = 10 – 150 cm^3/min) as shown in Figure 9a (Jo_2 = 3.7 $cm^3/min{\cdot}cm^2$). For this condition, a highly diluted product stream is obtained ($Co_{2,\ outlet}$ = 27%). A

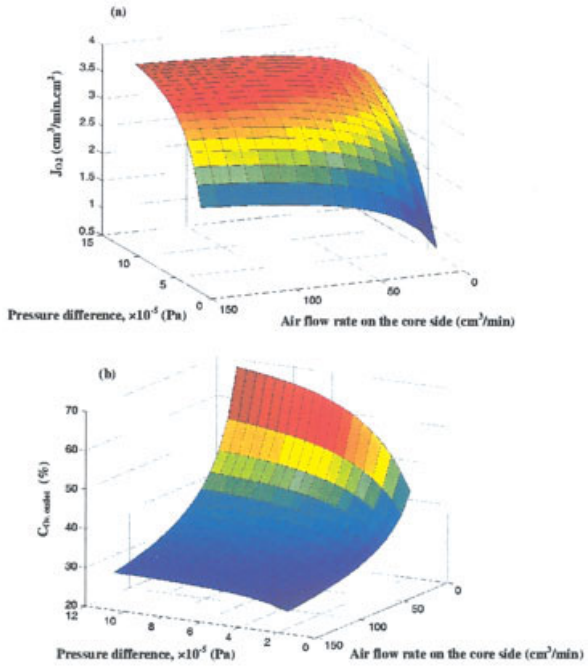

Figure 9. Influence of the pressure difference and air flow rate on the permeate side on the OEA production: oxygen permeation flux through the membrane (a) and the resulting O_2 concentration in the permeate stream (b).

Air flow rate: Feed side = 100 cm^3/min; permeate side = 10 – 150 cm^3/min, T = 950°C, pressure difference = 1.5 – 10 × 10^5 Pa. [Color figure can be viewed in the online issue, which is available at www.interscience.wiley.com.]

maximal O_2 concentration of about 68% was reached at T = 950°C for a pressure difference of 10 × 10^5 Pa at the lowest sweep gas flow rate (10 cm^3/min). Already for a more moderate pressure difference of 6.0 × 10^5 Pa (reduced costs for compression), a remarkable O_2-enrichment of about 60% can be obtained. Such operation condition characterized by small flow rates and without application of inert sweep gases can be of interest for compact small scale units like for medical applications (for example, artificial respiration). There is a second operation window related to higher oxygen permeation fluxes (as given, for example, for a permeate flow rate of 150 cm^3/min and a pressure difference of 10 × 10^5 Pa). The latter is more interesting if separable inert gas, for example steam, can be used as sweep gas. Thus, the dilution of the separated oxygen is not restricted.

Conclusions

Gastight BCFZ hollow fiber membranes have been prepared by phase inversion spinning followed by sintering. The prepared BCFZ hollow fiber membranes were employed for high temperature O_2-enrichment in air. The O_2 concentration reached in the experiments was approximately 55% corresponding with a production rate, OEA, of 5.2 cm^3/min·cm^2 at 950°C and a flow rate of 10 cm^3/min on the permeate side using a moderate total pressure difference of 3 × 10^5 Pa was obtained. Higher O_2 concentrations and production rates required for different industrial processes can be achievable by controlling the operational parameters, such as temperature, total pressure difference, gas flow rates. A mathematical model was developed to simulate the oxygen enrichment achievable using hollow fiber membranes. The theoretical results are in good agreement with experimental data. Based on the validated model of the air separation process, the mass-transfer properties of the membrane were calculated in a parameter range. The highest achievable amount of oxygen enrichment of about 68% was estimated for a temperature of 950°C, a pressure difference of 10 × 10^5 Pa and a flow rate of 10 and 150 cm^3/min on the permeate and retentat sides, respectively. The BCFZ perovskite hollow fiber membrane was steadily operated for more than 800 h for oxygen enrichment without any fracture. The long-time stability finding in our experiments indicates that the perovskite membrane of the type investigated has the potential to replace the current O_2-enrichment system for high temperature applications.[15]

Acknowledgment

The authors gratefully acknowledge the financial support of the German BMBF for project 03C0343A under the auspices of ConNeCat.

Notation

$C_{O_2,outlet}$ = O_2 concentration at the outlet on the core side, %
$C_{O_2,inlet}$ = fed O_2 concentration in air, %
D_{eff} = effective diffusion coefficient, cm^2/min·Pa^n
D_∞ = preexponential factor, cm^2/min·Pa^n
E_A = activation energy, kJ/mol
$F_{air,\ inlet}$ = fed air flow rate on the shell side, cm^3/min
F_{outlet} = O_2-enriched air flow rate of the outlet on the shell side, cm^3/min
i = component index
j = reaction index
J_{O_2} = oxygen permeation flux, cm^3/min·cm^2
J_i = flux of component i through hollow fiber, mol/s·cm^2
L = effective membrane length, cm
M = number of reactions
n_i^{ss} = molar flow rate of component i on the shell side, mol/s
n_{tot}^{ss} = total molar flow rate of component i on the shell side, mol/s
n_i^{cs} = molar flow rate of component i on the core side, mol/s
n_{tot}^{cs} = total molar flow rate of component i on the core side, mol/s
N = number of components
$P_{O_2}^{cs}$ = O_2 partial pressure on the core side, Pa
P_{tot}^{cs} = total pressure on the core side, Pa
$P_{O_2}^{ss}$ = O_2 partial pressure on the shell side, Pa
P_{tot}^{ss} = total pressure on the shell side, Pa
r = radial coordinate, cm
r_1 = inner radius of the hollow fiber membrane, cm
r_2 = outer radius of the hollow fiber membrane, cm
$\bar{r}$ = reaction rate, mol/g.s
R = radius of the ceramic tube as the shell, cm
R_{OEA} = O_2-enriched air production rate, cm^3/min·cm^2
S = effective membrane surface area, cm^2
t = the thickness of the hollow fiber, cm
ν_{ij} = stoichiometric coefficient for component i in the reaction j
ρ_{Bulk} = density of catalyst bed, g/cm3
z = axial coordinate, cm

Literature Cited

1. Bhasin DP, Liebeison MS, Chapman GJ. Oxygen increases FCC throughput. *Hydrocarbon Process.* 1983;62:85-88.
2. Baker R. Membrane Technology in the Chemical Industry: Further directions. in: Nunes S P, Peinemann KV. *Membrane Technology in the Chemical Industry*. Wiley-VCH; 2001.
3. Spillman R. Economics of gas separation membrane processes. in: Noble RD, Stern S A. *Membrane Science and Technology Series, 2*. Elsevier; 1996.

4. Tan XY, Liu YT, Li K. Mixed conducting ceramic hollow-fiber membranes for air separation. *AIChE J*. 2005;51:1991-2000.
5. Tan XY, Liu YT, Li K. Preparation of LSCF ceramic hollow-fiber membranes for oxygen production by a phase-inversion/sintering technique. *Ind Eng Chem Res.* 2005;44:61-66.
6. Tan XY, Liu SM, Li K. Preparation and characterization of inorganic hollow fiber membranes. *J Membr Sci.* 2001;88:87-95.
7. Liu SM, Tan XY, Li K, Hughes R. Preparation and characterisation of $SrCe_{0.95}Yb_{0.05}O_{2.975}$ hollow fiber membranes. *J Membr. Sci.* 2001; 193:249-260.
8. Liu SM, Li K, Hughes R. Preparation of $SrCe_{0.95}Yb_{0.05}O_{3-\delta}$ perovskite for use as a membrane material in hollow fiber fabrication. *Mater Res Bull.* 2004;39:119-133.
9. Liu SM, Gavalas GR. Oxygen selective ceramic hollow fiber membranes. *J Membr Sci.* 2005;246:103-108.
10. Liu SM, Gavalas GR. Preparation of oxygen ion conducting ceramic hollow-fiber membranes. *Ind Eng Chem Res*. 2005;44:7633-7637.
11. Schiestel T, Kilgus M, Peter S, Caspary KJ, Wang H, Caro J. Hollow fiber perovskite membranes for oxygen separation. *J Membr Sci.* 2005;258:1-4.
12. Trunec M. Fabrication of zirconia- and ceria-based thin-wall tubes by thermoplastic extrusion. *J Eur Ceram Soc.* 2004;24:645-651.
13. Luyten J, Buekenhoudt A, Adriansens W, Cooymans J, Weyten H, Servaes F, Leysen R. Preparation of $LaSrCoFeO_{3-x}$ membranes. *Solid State Ionics.* 2000;135:637-642.
14. Tablet C, Grubert G, Wang HH, Schiestel T, Schroeder M, Langanke B, Caro J. Oxygen permeation study of perovskite hollow fiber membranes. *Catal Today*. 2005;104:126-130.
15. Wang HH, Werth S, Schiestel T, Caro J. Perovskite hollow fiber membranes for the production of O_2-enriched air. *Angew Chem Int Ed*. 2005;44:6906-6909.
16. Tsai CY, Dixon AG, Moser WR, Ma YH. Dense perovskite membrane reactors for the partial oxidation of methane to syngas. *AIChE J*. 1997;43:2741-2750.
17. Balachandran U, Dusek JT, Maiya PS, Ma B, Mieville RL, Kleefisch MS, Udovich CA. Ceramic membrane reactor for converting methane to syngas. *Catal Today*. 1997;36:265-272.
18. Bouwmeester HJM. Dense ceramic membranes for methane conversion. *Catal. Today*. 2003;82:141-150.
19. Gu XH, Jin WQ, Chen CL, Xu NP, Shi J, Ma YH. YSZ-$SrCo_{0.4}Fe_{0.6}O_{3-\delta}$ membranes for the partial oxidation of methane to syngas. *AIChE J*. 2002;48:2051-2060.
20. Xu SJ, Thomson WJ. Perovskite-type oxide membrane for the oxidative coupling of methane. *AIChE J*. 1997;43:2731-2740.
21. Elshof JE, Bouwmeester HJM, Verweij H. Oxidative coupling of methane in a mixed-conducting perovskite membrane reactor. *Appl Catal General: A*. 1995;130:195-212.
22. Akin FT, Lin YS. Oxidative coupling of methane in dense ceramic membrane reactor with high yields, *AIChE J*. 2002;48:2298-2306.
23. Wang HH, Cong Y, Yang WS. High selectivity of oxidative dehydrogenation of ethane to ethylene in an oxygen permeable membrane reactor. *Chem Commun*. 2002;14:1468-1469.
24. Rebeilleau-Dassonneville M, Rosini S, van Veen AC, Farrusseng D, Mirodatos C. Oxidative activation of ethane on catalytic modified dense ionic oxygen conducting membranes. *Catal Today*. 2005;104: 131-137.
25. Akin FT, Lin YS. Selective oxidation of ethane to ethylene in a dense tubular membrane reactor. *J Membr Sci*. 2002; 209:457-267.
26. Ren JY, Fan YQ, Egolfopoulos FN, Tsotsis TT. Membrane-based reactive separations for power generation applications: oxygen lancing. *Chem Eng Sci*. 2003;58:1043-1052.
27. Fan YQ, Ren JY, Onstot W, Pasale J, Tsotsis TT, Egolfopoulos FN. Reactor and technical feasibility aspects of a CO_2 decomposition-based power generation cycle, utilizing a high-temperature membrane reactor. *Ind Eng Chem Res.* 2003;42:2618-2626.
28. Teraoka Y, Zhang HM, Furukawa S, Yamazoe N. Oxygen permeation through perovskite-type oxides. *Chem Lett.* 1985;11:1743-1746.
29. Wang HH, Wang R, Liang DT, Yang WS. Experimental and modeling studies on $Ba_{0.5}Sr_{0.5}Co_{0.8}Fe_{0.2}O_{3-\delta}$ (BSCF) tubular membranes for air separation. *J Membr Sci.* 2004;243:405-415.
30. Gellings PJ, Bouwmeester HJM. *The CRC Handbook of Solid State Elektrochemistry*. CRC Press; 1997.
31. Wagner C, Schottky W. Beitrag zur Theorie des Anlaufvorganges. *Z Phys Chem*. 1930;B11:25-41.
32. Wagner C. Equations for transport in solid oxides and sulfides of transition metals. *Prog Solid State Chem.* 1975;10(1):3-16.
33. Redfern D, Campbell C. The Matlab 5 Handbook. Springer; 1997
34. Matson SL, Ward WJ, Kimura SG, Browall WR. Membrane oxygen enrichment. 2. Economic assessment. *J Membr Sci.* 1986;29:79-96.
35. Budd PM, McKeown NB, Fritsch D. Free volume and intrinsic microporosity in polymers. *J Mater Chem*. 2005;15:1977-1986.

Manuscript received Feb. 3, 2006, and revision received May 31, 2006.